Asian Journal of Chemistry; Vol. 37, No. 11 (2025), 2679-2688
ASIAN JOURNAL OF CHEMISTRY
https://doi.org/10.14233/ajchem.2025.34513

Synthesis of Zirconium-Doped ZnO Nanoparticles using *Grewia optiva* for Environmental Sensing of Heavy Metal Ions

SHIVANI RAUTHAN*, AJAY SINGH and RITU PAINULI

School of Applied and Life Sciences, Uttaranchal University, Dehradun-248007, India

*Corresponding author: E-mail: rauthanshivani05@gmail.com

Received: 22 August 2025 *Accepted*: 8 September 2025 *Published online*: 27 October 2025 AJC-22154

The purpose of this work was to synthesize zinc oxide nanoparticles (ZnONPs) using leaf extract of *Grewia optiva*. The prepared nanoparticles were further doped with zirconium. The UV-vis analysis of green synthesized ZnONPs showed peaks at a wavelength of 239 nm, whereas after doping by Zr^{4+}, a peak was observed at 230 nm, demonstrating a hypsochromic shift, which confirms doping of Zr^{4+} onto ZnONPs. A comparison was done between ZnONPs and Zr-doped ZnONPs at different concentrations of toxic metals and the results showed that Zr-doped ZnONPs showed better selectivity towards Pb^{2+} ions. When examined using a Saryu River water sample, the Zr-doped ZnO nanoparticles demonstrated significant sensitivity to Pb^{2+} ions, emphasizing their suitability as light-responsive catalyst for sensing heavy metal ions.

Keywords: Green synthesis, *Grewia optiva*, Zinc oxide, Nanoparticles, Zirconium, Doping.

INTRODUCTION

Although zinc oxide (ZnO) naturally occurs as zincite, it is mainly synthesized for commercial use due to its low cost, non-toxicity, antibacterial properties, strong piezoelectricity, deodorizing effect and biocompatibility. These features make ZnO ideal for applications in textiles, rubber and food packaging [1]. ZnO exhibits strong n-type conductivity due to low energy native point defects. With a wide bandgap of 3.36 eV and a high exciton binding energy of 60 meV at room temperature, it is a versatile semiconductor suitable for applications in UV-visible optoelectronics, lasers, electromagnetic sensors and surface acoustic wave devices [2,3]. Other notable uses of ZnO are in microelectronics, biomolecular detection and diagnostics. ZnONPs are capable of degrading arsenic, cadmium and selenium in water [4-6].

ZnONPs have several biomedical applications, including antibacterial anticancer, antidiabetic, anti-inflammatory activities, drug delivery and bioimaging activity [7]. Nonetheless, doping elements are utilized to synthesize new, alluring properties, involving light-emitting diodes, solar cells, flat panel displays, surface acoustic wave devices and transparent electrodes [8]. Doping ZnO with transition metals can significantly enhance its photocatalytic efficiency, primarily due to the presence of unoccupied *d*-orbitals in these metals, which facilitate charge transfer processes [9]. Moreover, the comparable atomic radii of these dopants to Zn^{2+} allow their effective incorporation into the ZnO crystal lattice without substantial structural distortion [10]. Zirconium, an n-type dopant, does not exhibit inherent antibacterial activity; however, when used to dope ZnO nanoparticles, it markedly improves their antimicrobial performance [11]. This enhancement is attributed to Zr's ability to modulate the release of Zn^{2+} ions, thereby increasing interaction with the microbial cells and amplifying antibacterial efficacy [12]. Notably, the ionic radius of Zr^{4+} (0.84 Å) is slightly larger than that of Zn^{2+} (0.74 Å), enabling Zr to substitute Zn in the lattice while inducing lattice strain, which can further tune the material's properties. Consequently, Zr-doping not only boosts the antibacterial capabilities of ZnO nanoparticles but also enhances their potential for optoelectronic applications due to improved charge carrier dynamics and structural modifications [13,14].

The incorporation of nanomaterials in sensors has accomplished an improvement in selectivity, on-site detection ability and sensitivity for heavy metals [15]. Zr doping on ZnO enhances its performance in sensing devices [16,17], but the mechanisms behind this improvement remain underexplored. Phytogenic or green synthesis, which uses plant extracts, offers

several advantages, including the incorporation of bioactive compounds like proteins, flavonoids and polyphenols that improve the biological activity of nanoparticles [18,19]. *Grewia optiva*, a Tiliaceae family plant found in India and Nepal, is known for its antioxidant, antibacterial and therapeutic activities [20]. Traditionally used for animal feed, fiber and medicine, its bark and leaves contain compounds like grewialin, sitosterol and lupeol, along with functional groups such as carboxyl, amino and hydroxyl, making it effective in metal binding and nanoparticles synthesis [21,22].

The present study focuses on the green synthesis of zinc oxide nanoparticles (ZnONPs) using *Grewia optiva* aqueous leaf extract, leveraging the plant's inherent antibacterial properties to impart bioactivity to the nanoparticles. To further enhance their functional performance, the ZnONPs were doped with zirconium (Zr), which significantly improved their antibacterial efficacy, electrical conductivity and sensing capabilities. Comprehensive characterization techniques, including UV-Vis spectroscopy, scanning electron microscopy (SEM), X-ray diffraction (XRD), energy-dispersive X-ray spectroscopy (EDX) and Fourier-transform infrared spectroscopy (FTIR), were employed to analyze the structural and morphological features of both undoped and Zr-doped ZnONPs. Moreover, the Zr-doped ZnONPs were successfully applied for the detection of toxic heavy metals in water samples collected from the Saryu River, Ayodhya city, demonstrating their potential as efficient photosensitive material in the environmental monitoring applications.

EXPERIMENTAL

All chemicals used were obtained from HiMedia Laboratories, India. *Grewia optiva* was collected in February 2025, from the district of Tehri Garhwal. The water sample of Saryu River was collected from Ayodhya city, India.

Characterization: The UV-Vis absorption spectra were measured by using a LabMan UV-vis Spectrophotometer-UV1900, covering the wavelength range of 200-800 nm. The FTIR analysis was conducted through Nicolet Summit Lite utilizing a Hitachi S3400 instrument using the KBr pellet method. The phase structure and material identity were examined using PANalytical system using Cu*K*α X-ray diffractometer under room temperature. SEM and EDX analyses were conducted using Zeiss EVO 18 to observe the particle's size and shape and to analyze the elemental composition of the prepared NPs, respectively.

Aqueous leaf extract of *G. optiva*: *G. optiva* leaves (20 g) were washed multiple times with tap water to remove the surface contaminants, followed by two-three times washing with deionized water to eliminate the residual impurities. The leaves were shade-dried for 30 days and subsequently ground into a fine powder using a mortar and pestle. Approximately 20 g of the powdered leaves were transferred to a conical flask containing 200 mL of deionized water. The mixture was heated at 80 °C for 4 h under continuous stirring, then allowed to cool to room temperature. The resulting solution was filtered using Whatman No. 1 filter paper and the filtrate was stored in a cool, dark place until further use.

Preparation of ZnONPs: Zinc nitrate hexahydrate (1 g) was dissolved in 100 mL distilled water and stirred constantly at room temperature. Then 2 mL of aqueous extract of *G. optiva* leaves was added to it with constant stirring. The final product was collected after centrifuging thrice at 5000 rpm for 15 min while washing with distilled water. The synthesized nanoparticles were dried and stored at room temperature for further examination.

Doping of zirconium in ZnONPs: To carry out the doping process, zirconyl nitrate hydrate (0.4 g) was dissolved in 100 mL of distilled water and stirred continuously until the solution became homogenous and clear. Then, 2 g of prepared ZnONPs were introduced into the solution and stirred consistently to achieve proper mixing. The mixture was centrifuged three times at 5000 rpm for 10 min each time, with washing steps using distilled water to eliminate any remaining impurities. The resulting Zr-doped ZnO nanoparticles were collected, dried and stored at ambient temperature for subsequent use.

Colorimetric detection of toxic metals: The colorimetric detection of toxic metals by using the prepared ZnONPs solution was achieved by mixing 100 ppm of Pb^{2+}, Cr^{6+}, Cr^{3+}, Hg^{2+}, As^{3+}, Cd^{2+}, Ni^{2+}, Ca^{2+}, Mg^{2+}, KCl and Cu^{2+} metal ion solutions into 50 ppm of ZnONPs solution. The applicability of the prepared Zr-doped ZnONPs was also conducted by using a 50 ppm prepared Zr-doped ZnONPs solution to 10 ppm of metal ion solutions. Similar tests were conducted on the Saryu River water sample to assess the applicability of the Zr-doped ZnONPs as a sensor for metal detection.

Sensing of toxic metals: In this study, aqueous solutions of various metal ions including Pb^{2+}, Cr^{6+}, Cr^{3+}, Hg^{2+}, As^{3+}, Cd^{2+}, Ni^{2+}, Ca^{2+}, Mg^{2+}, Cu^{2+} and KCl were prepared at concentrations of 100 ppm and 0.1 ppm using deionized water. Each of these metal ion solutions was individually mixed with a 100 ppm suspension of Zr-doped ZnONPs to investigate their interaction *via* UVvisible absorption spectroscopy [23]. The same protocol was applied to a water sample collected from the Saryu River, in order to evaluate the sensing capabilities of the synthesized nanoparticles under real environmental conditions.

RESULTS AND DISCUSSION

UV-visible studies: Fig. 1a shows a prominent peak at the wavelength of 239 nm, which confirms the presence of ZnO [24,25]. As shown in the inset of Fig. 1a, the Tauc plot of the control sample indicates a direct band gap energy of 3.86 eV. In comparison, the Tauc plot in Fig. 1b (inset) corresponds to ZnONPs, exhibiting an indirect band gap of 3.58 eV. Upon doping with zirconium, the UV-vis absorption spectrum of Zr-doped ZnONPs (Fig. 1c) displays a pronounced absorption peak at 230 nm, indicating a hypsochromic (blue) shift relative to undoped ZnONPs, which aligns with observations reported by Gouthamsri *et al*. [26]. Furthermore, the Tauc plot of the Zr-doped ZnONPs (Fig. 1c inset) reveals a reduced direct band gap of 3.12 eV. This narrowing of the band gap is consistent with findings from Ibrahim *et al*. [27] and suggests that Zr incorporation effectively alters the electronic structure of ZnO, potentially enhancing its optoelectronic properties for sensing and photocatalytic applications.

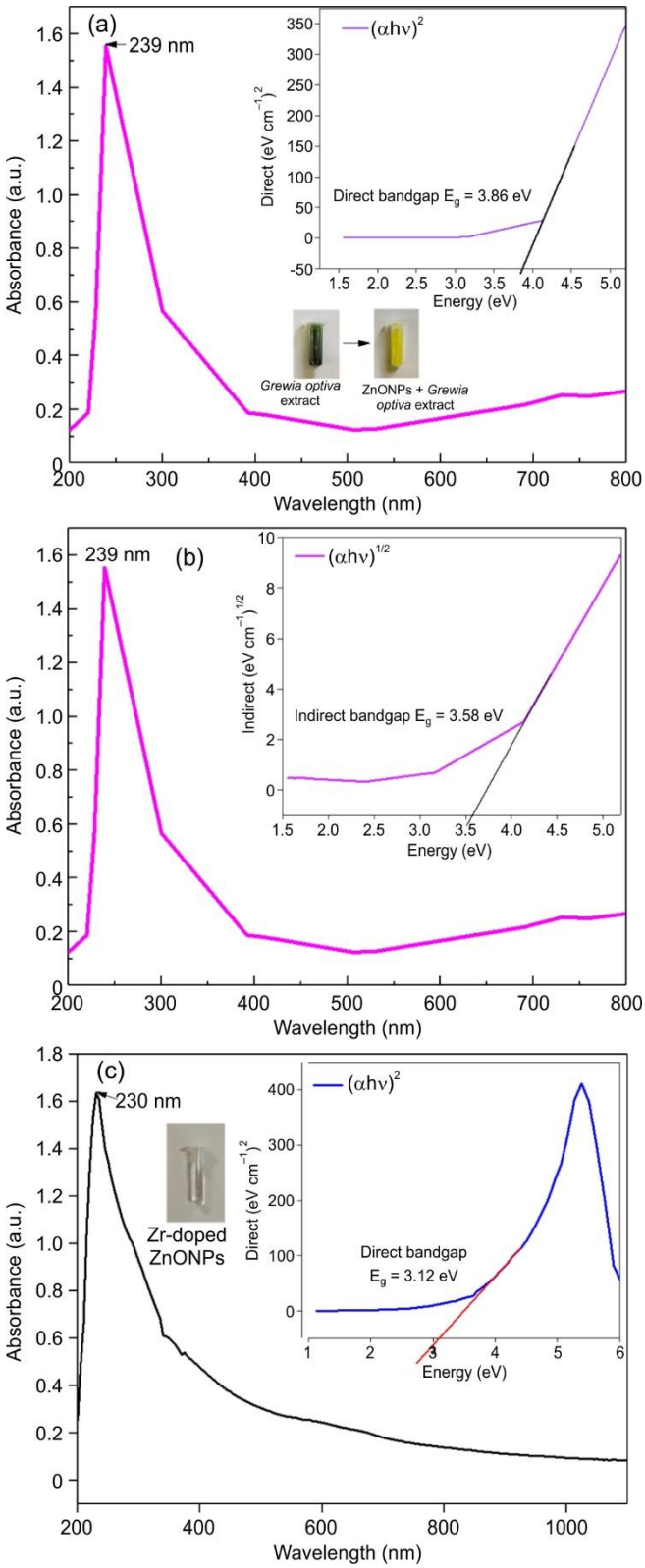

Fig. 1. (a) UV-vis spectra of (a) ZnONPs with inset Tauc plot showing direct bandgap, (b) ZnONPs with inset Tauc plot showing indirect bandgap, and (c) Zr-doped ZnONPs with inset Tauc plot showing direct bandgap

SEM studies: The surface morphology of the synthesized nanoparticles was examined using SEM analysis. As shown in Fig. 2a, the ZnONPs exhibit a predominantly spherical shape, with a tendency to cluster and form bundled structures. This agglomeration is attributed to the inherent polarity and electrostatic interactions among the ZnONPs [28,29]. In contrast, the SEM image presented in Fig. 2b reveals distinct morphological changes upon zirconium doping. The spherical ZnO particles appear elongated and transform into bullet-like structures with a more irregular distribution, consistent with the findings reported by Khan *et al.* [30]. The average particle size of the undoped ZnONPs was measured to be 14.74 nm, while the Zr-doped ZnONPs exhibited a slightly reduced size of 14.04 nm. This reduction in grain size indicates that Zr^{4+} ions act as effective grain growth inhibitors. The substitution of Zn^{2+} ions in the ZnO crystal lattice by Zr^{4+} occurs through chemical bonding during the doping process, thereby influencing both the morphology and size of the resulting nanoparticles.

EDX spectrum: The EDX spectrum of ZnONPs are shown in Fig. 3a, confirming 40.2% of Zn in the sample, whereas the EDX spectrum in Fig. 3b indicate the presence of both Zn and Zr in the sample, specifically Zr-doped-ZnONPs (Zn = 35.03% and Zr = 7.14%).

FT-IR spectral studies: The prepared ZnONPs were subjected to FTIR spectroscopy to analyze their composition and to identify the phytochemicals present in the extract, as well as the type and purity of the prepared nanoparticles. Zinc interacting with phytochemicals such as carboxylic acids, amines, phenols and alcohols can help in stabilizing the ZnNPs. The FTIR band in the range of 827 cm^{-1} is due to Zn-O vibration [31,32].

Fig. 4a shows a comparison of the FT-IR spectrum of aqueous leaf extract of *G. optiva* and synthesized ZnONPs. The absorption band at 3420 cm^{-1} confirms the presence of stretching vibration of the phenol and hydroxyl group [33], whereas the absorption band at 2906 cm^{-1} is due to the stretching of the C-H group in the glucose unit [34]. The absorption bands at 2833 cm^{-1} and 2766 cm^{-1} indicate the presence of aldehydes in the sample. The bands at 2428 cm^{-1} and 2396 cm^{-1} are assigned to C=O and P-O-H stretching vibrations, respectively [35,36]. The absorption band observed at 1763 cm^{-1} is attributed to the C=C stretching vibrations, which may be associated with aromatic conjugated systems present in the biomolecules of the plant extract. The peak at 1628 cm^{-1} confirms the presence of amides or carboxylate functional groups. The absorption band at 1358 cm^{-1} corresponds to the presence of phenolic groups or *tertiary* alcohols. The characteristic C–O stretching vibration of alcohols is observed at 1053 cm^{-1}. The band at 960 cm^{-1} is attributed to *trans* C–H out-of-plane bending vibrations. A prominent peak at 827 cm^{-1} confirms the presence of Zn–O bonds, as reported in previous studies [37]. The appearance of this additional band at 827 cm^{-1} in the FTIR spectrum of the ZnONPs synthesized using the plant extract suggests successful formation of ZnONPs, with plant biomolecules likely playing a role in the reduction and stabilization processes.

As shown in Fig. 4b, the intense absorption bands in 468-404 cm^{-1} region indicate stretching of the ZnO bond. Close to the FT-IR results of Azam *et al.* [38], in this study, a characteristic peak at 468 cm^{-1} indicates the Zn-O modes and therefore confirms the formation of ZnO bands in Zr-doped

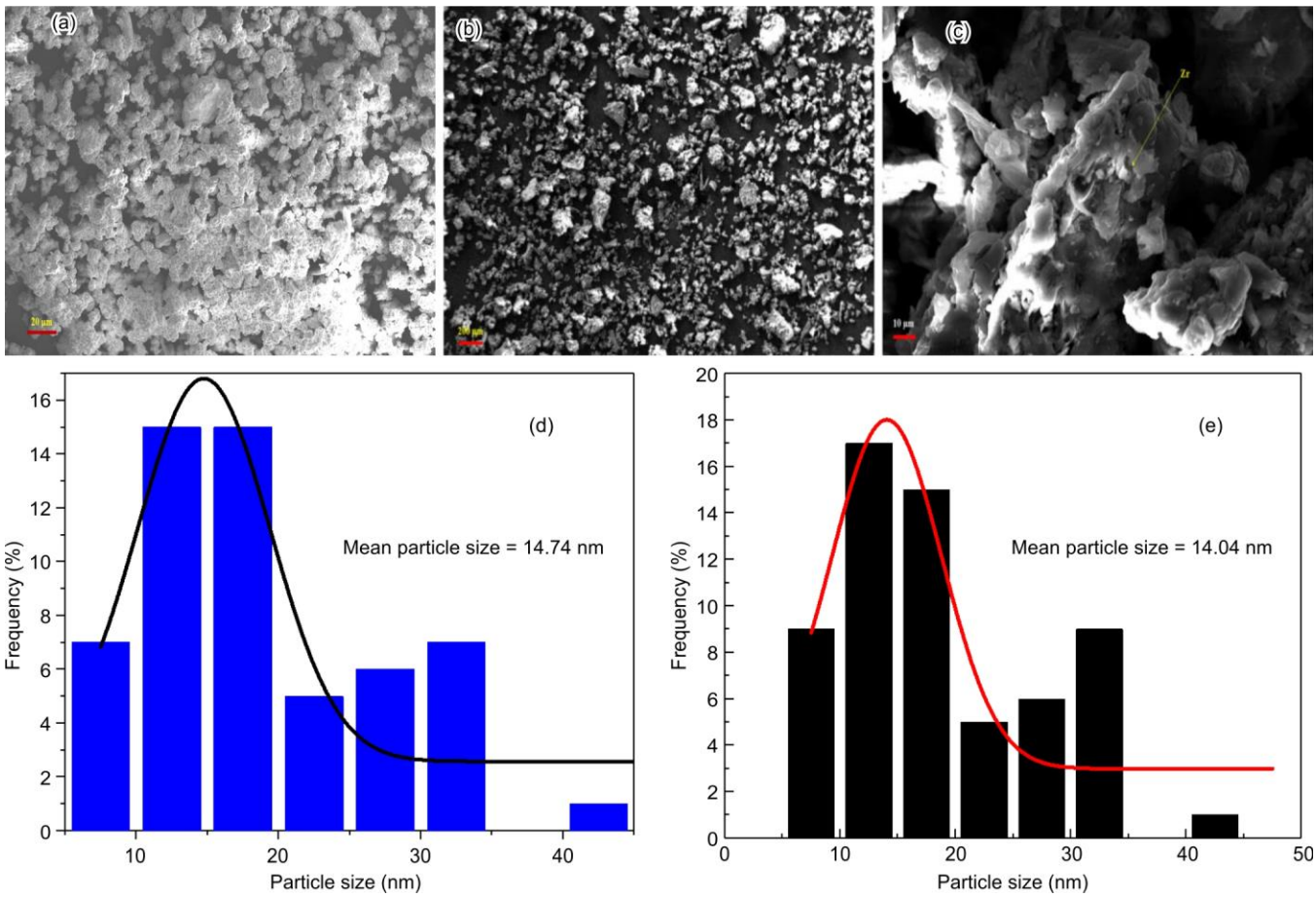

Fig. 2. SEM images of (a) ZnONPs, (b) Zr-doped ZnONPs and Zr-doped ZnONPs; (d) Particle distribution graphs of ZnONPs and (e) Zr-doped ZnONPs

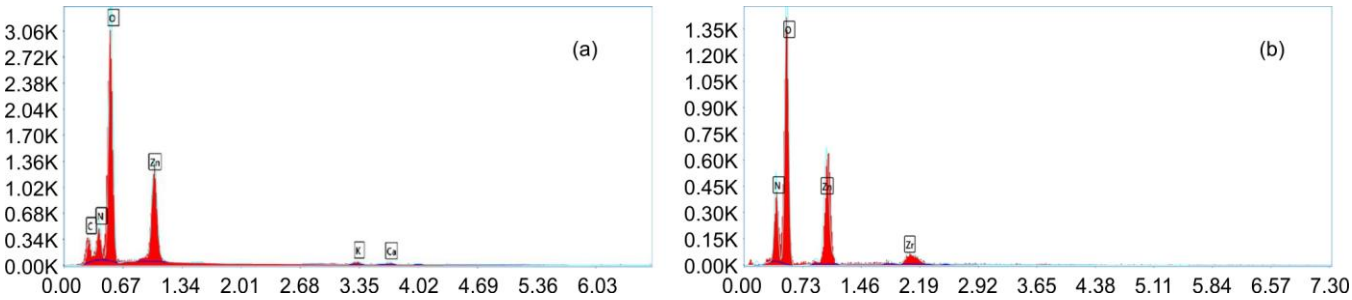

Fig. 3. EDX spectra of (a) ZnONPs and (b) Zr-doped ZnONPs

ZnONPs. Absorption band at 454 cm^{-1} shows Zr-O_2-Zr bond, which is close to the results of Patel *et al.* [39]. The peaks in the range 850-500 cm^{-1} indicated ZrO bond [40], whereas the peak at 861 cm^{-1} indicates that after doping with Zr, the ZnO peak shifted to a lower wavenumber. This shift reveals the replacement of the Zr ion into the Zn-O lattice. This shift in the position of the ZnO absorption band on doping by Zr may be due to a variation in bond length as Zr replaces Zn. There may be a backward shift of the transverse optical photon mode due to the heavier mass of Zr than that of Zn. Naik *et al.* [41] and Murtaza *et al.* [42] also observed a similar shift in the IR absorption band after doping by Zr on ZnO. Moreover, the absorption band at 943 cm^{-1} and the band around 3452 cm^{-1} represent O-H stretching in water [41,43]. The peaks ranging from 1812 cm^{-1} and 2072 cm^{-1} may reflect traces of CO_2 on the surface of Zr-doped-ZnONPs [41].

XRD studies: As illustrated in Fig. 5a, the diffraction peaks corresponding to various lattice planes confirm that the synthesized ZnO nanoparticles possess a hexagonal wurtzite crystal structure. The calculated lattice parameters for ZnONPs, presented in Table-1, yield a *c/a* ratio of 1.60, which is consistent with the ideal hexagonal geometry. Similarly, the XRD pattern of the Zr-doped ZnONPs (Fig. 5b) also exhibits the diffraction peaks characteristic of the hexagonal wurtzite phase, as verified by standard reference data (JCPDS card No. 36-1451) [43]. A prominent diffraction peak observed at 2θ = 29.58°, corresponding to the (001) plane, further supports this phase identification. The lattice parameters of Zr-doped ZnONPs

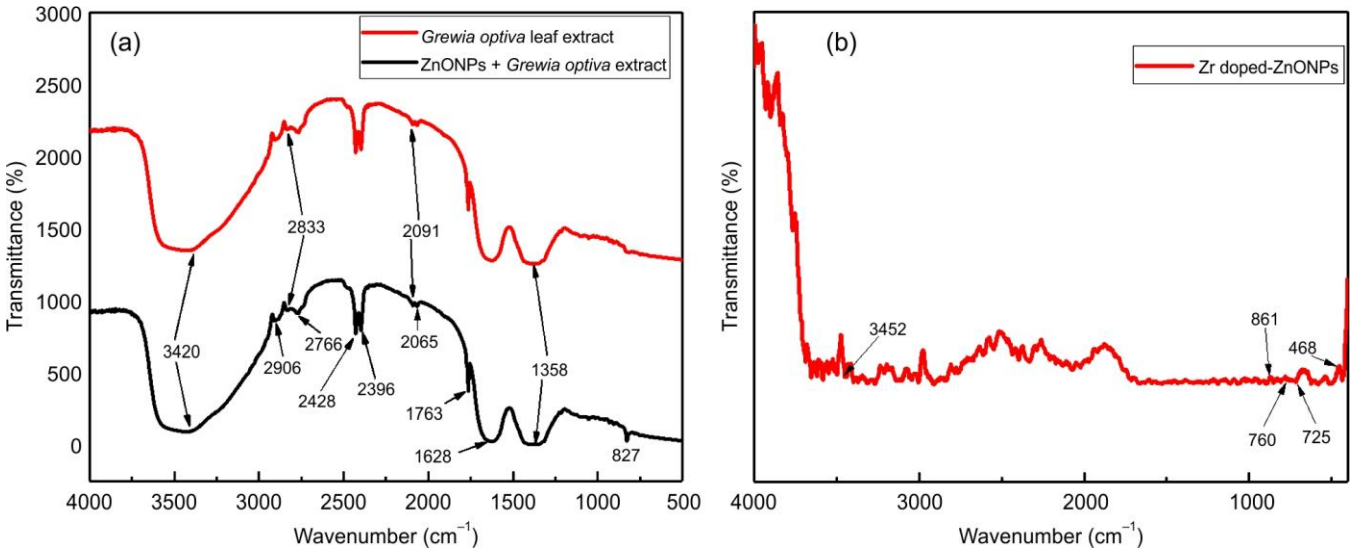

Fig. 4. (a) FTIR spectra of *G. optiva* aq. leaf extract and as-synthesized ZnONPs mediated through *G. optiva* aq. leaf extract; (b) FTIR spectrum of Zr-doped ZnONPs

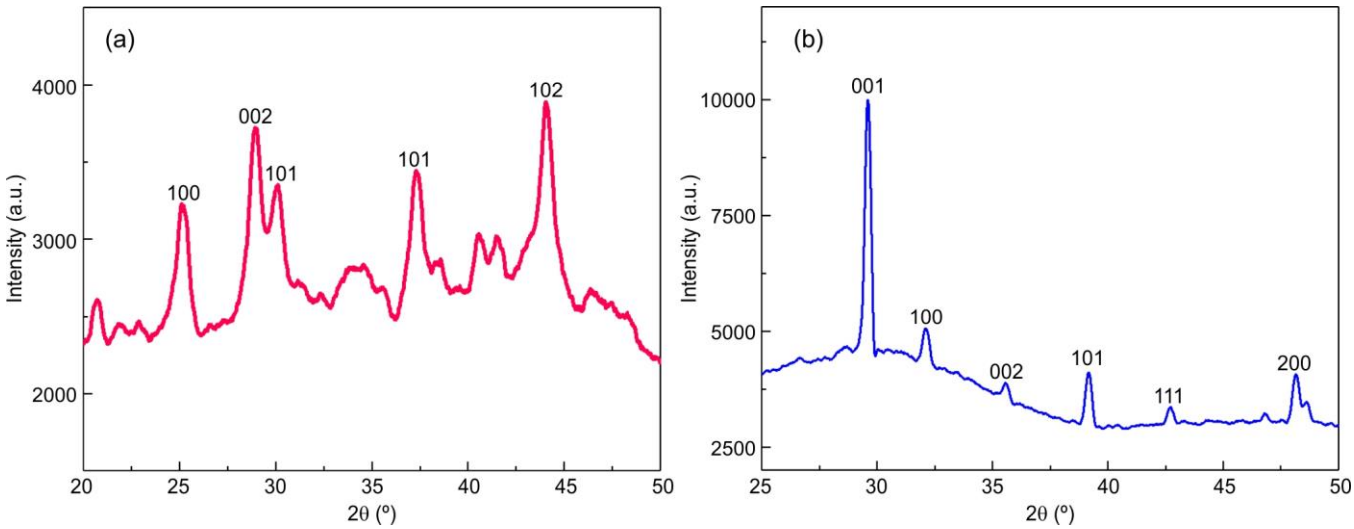

Fig. 5. (a) XRD spectra of ZnONPs and (b) Zr-doped ZnONPs

indicate that Zr incorporation does not alter the crystal structure significantly (Table-1), but may slightly influence lattice dimensions due to ionic substitution. The crystalline size was evaluated using Debye-Scherrer's formula as shown in eqn. 1 [44]:

TABLE-1
LATTICE PARAMETERS OF ZnONPs (Å)
AND Zr-DOPED ZnONPs (Å)

ZnONPs (Å)			Zr-doped ZnONPs (Å)		
Lattice parameters	a	c	Lattice parameters	a	c
100	3.53	–	001	–	3.01
002	–	6.16	100	3.23	–
101	3.50	5.60	002	–	5.04
101	2.83	4.54	101	5.47	3.35
102	3.28	5.25	111	6.75	4.14
			200	4.38	–

$$\gamma = \frac{0.89 \times \lambda}{\beta \cos\theta} \quad (1)$$

where γ is the crystallite size (nm); λ is the wavelength (λ = 1.54 nm); β is the full width at half maximum; and θ is the diffraction angle. The mean crystallite size for ZnONPs is 1.46 nm and for Zr-doped ZnONPs is 5.87 nm.

Selectivity test of synthesized ZnONPs: To examine the selectivity of ZnONPs towards various metal ions, 100 ppm of each metal ion solution was added into 50 ppm of ZnONPs solution. Upon the addition of various metal ions, namely Pb^{2+}, Cr^{6+}, Cr^{3+}, Hg^{2+}, As^{3+}, Cd^{2+}, Cu^{2+}, Ni^{2+} and other toxins like Mg^{2+}, Ca^{2+} and KCl, no significant change was observed. However, after the addition of Pb^{2+} ions change in colour was observed from yellow to transparent (precipitate was formed) (Fig. 6a). This was also supported by the change in the SPR spectra of ZnONPs along with metal ions. As shown in Fig. 6b, on the addition of heavy metal ions onto the ZnONPs, a dramatic change in the UV-vis peak of Pb^{2+} along with a

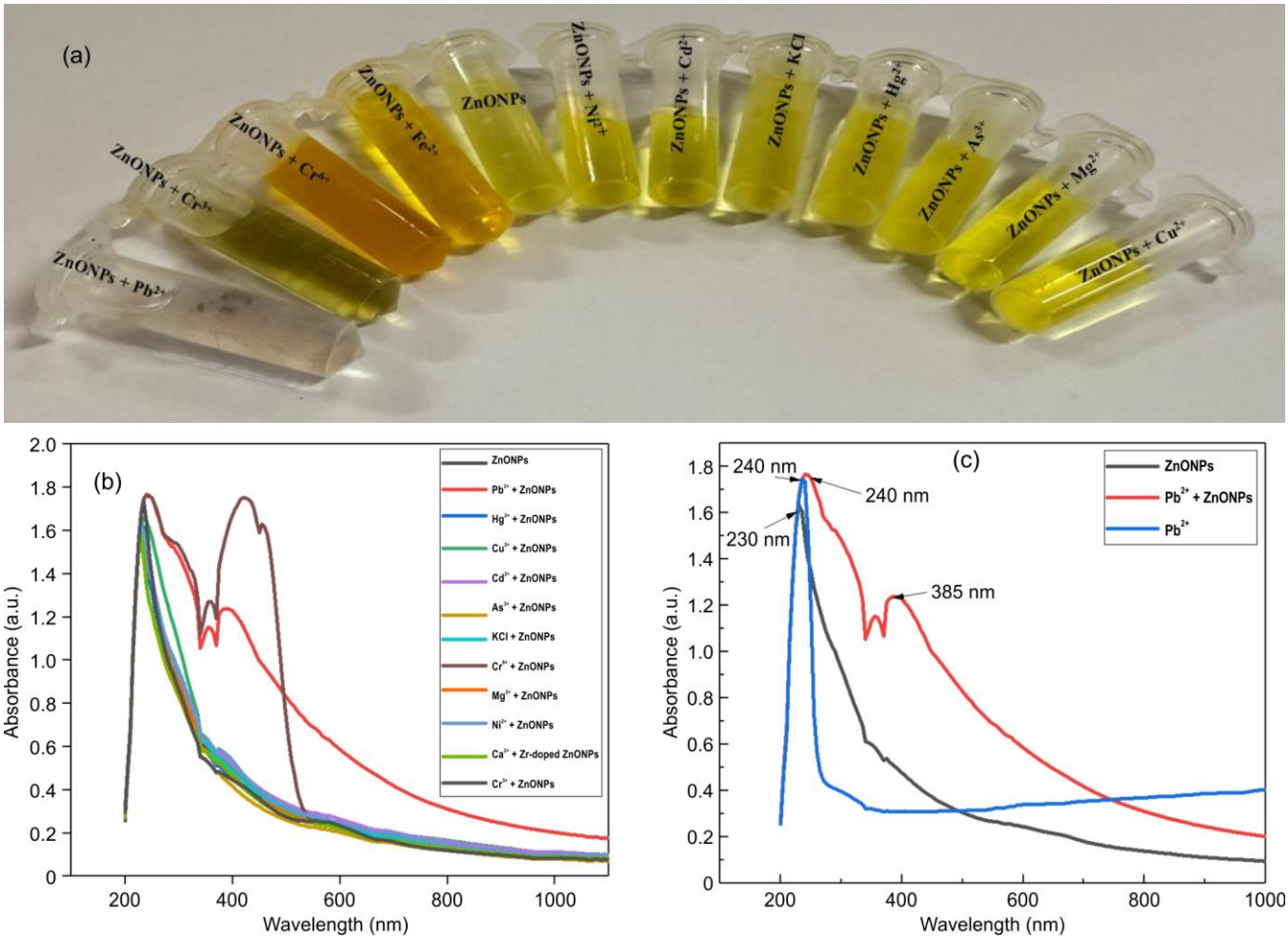

Fig. 6. (a) Colorimetric change of ZnONPs on the addition of heavy metals at 100 ppm; (b) UV-vis spectra of ZnONPs in the presence of various metal ions (100 ppm each); (c) UV-vis spectra of ZnONPs with and without Pb^{2+}

bathochromic shift at 240 nm and 385 nm was observed. Whereas, the spectrum of all other metal ions didn't show any major changes. Scrutinizing the performance of ZnONPs concerning various heavy metal ions was appraised by UV-visible absorption spectra, as shown in Fig. 6b. The discrete and sensitive variation in absorbance demonstrates the capability of ZnONPs to act as effective optical sensors, particularly in the UV and visible ranges. Lead ions, when they come in contact with ZnONPs, form a charge-transfer complex, which may lead to a bathochromic shift in the UV-vis spectrum as a result of the lowering of the bandgap (Fig. 6c) [45]. Similar tests were conducted for heavy metals at lower concentrations, but no significant changes were observed in the UV-vis spectrum; therefore, ZnONPs were unable to detect heavy metals at lower concentrations. Hence, Zr^{4+} doping was done to enhance the selectivity performance of ZnONPs. Doping Zr^{4+} on ZnONPs primarily increases the surface area of ZnONPs from 11.35 to 26.18 m^2/g, modifying structural and electronic properties, which carry the additional active sites for interaction with heavy metal ions, hence improving the sensitivity [46-48].

Selectivity test for Zr-doped ZnONPs: Fig. 7 displays the selectivity of Zr-doped ZnONPs toward various heavy metal ions. The sensing capability of Zr-doped ZnONPs towards heavy metal ions was observed *via* the naked eye on adding 10 ppm of each metal ion onto 50 ppm of the Zr-doped ZnONPs solution. The colorimetric changes on the addition of heavy metal ions onto the Zr-doped ZnONPs are shown in Fig. 7a. Here, on addition of Pb^{2+} to Zr-doped ZnONPs solution, formation of precipitate was observed, although no such changes were observed on the addition of Zr-doped ZnONPs to the other metal ions. This experiment was further encouraged by UV-vis spectroscopy as shown in Fig. 7b, where a dramatic change in the UV-vis peak of Pb^{2+} was recorded, with a hypsochromic and hypochromic shift at 225 nm [49]. Pb^{2+} is encircled by chloride ligands due to the presence of chloride in lead(II) chloride, forming Pb complexes [50]. On contact with the Zr-doped ZnONPs surface, these ions may be expatriate, leading to decrease polarizability and an increased energy gap between the ground and excited states, which might contribute to the hypsochromic shift. The *d–p* or *p–p* transitions of Pb^{2+} are delicate to the coordination geometry. Its surface adsorption on Zr-doped ZnONPs may establish a weaker ligand field relative to the free ion, shifting transitions to higher energy. If the new geometry leads to fewer permissible transitions, the absorbance drops, resulting in the hypochromic shift. Lead(II) ions strongly adsorbs onto Zr-doped ZnO, due to its Zr-induced surface defects and high surface

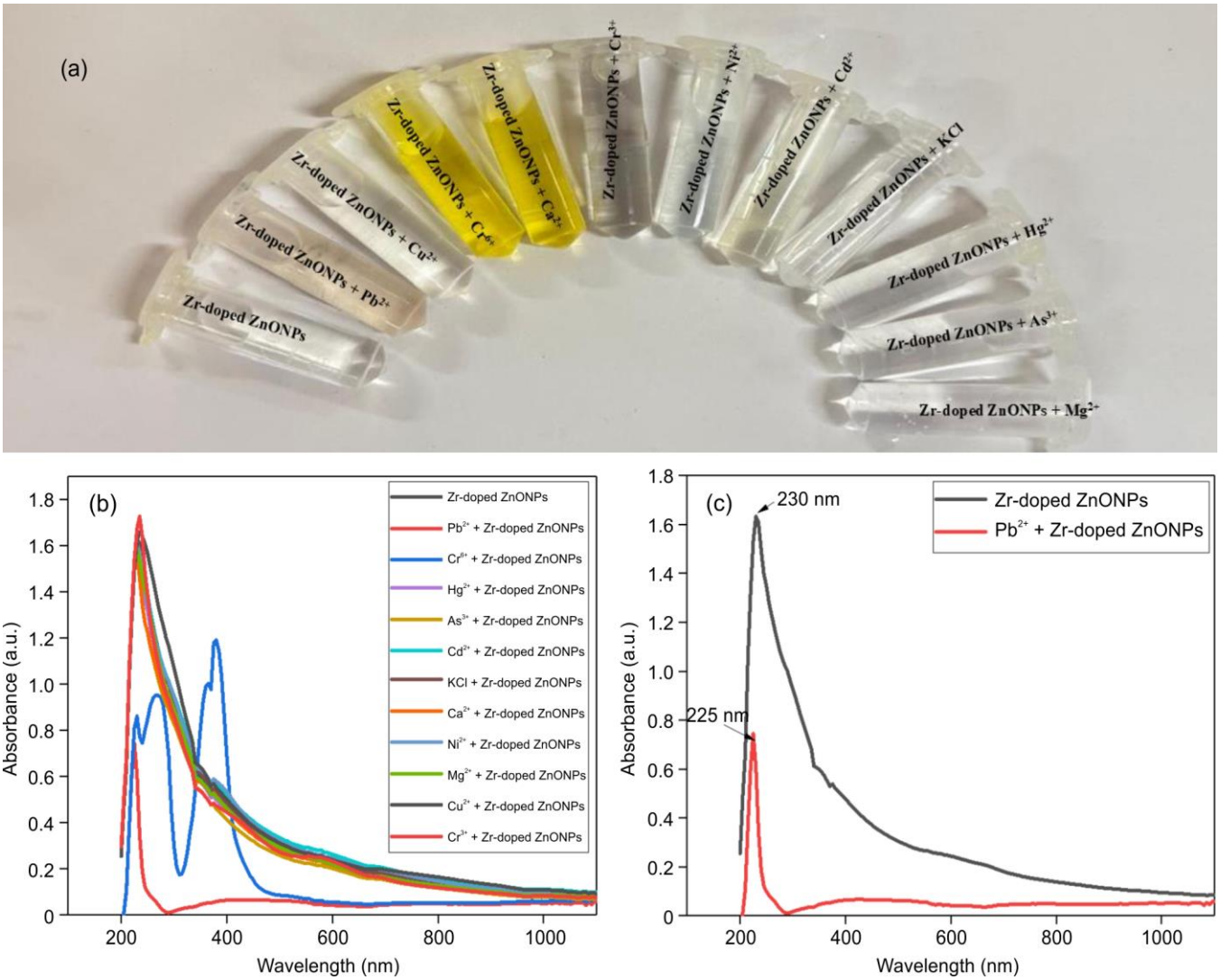

Fig. 7. Colorimetric change of Zr-doped ZnONPs on the addition of heavy metals at 0.1 ppm; (b) UV-vis spectrum of Zr-Doped ZnONPs in the presence of various metal ions (0.1 ppm each); (c) UV-vis spectrum of Zr-Doped ZnONPs with 0.1 ppm Pb^{2+}

area, resulting in inferior absorbance intensity [41] and therefore displaying a hypochromic effect. Table-2 summarizes the results of the conducted experiments. The spectrum of all other metal ions didn't shows any major changes.

To estimate the detection limit of Zr-doped ZnONPs, the sensitivity tests were also conducted as a function of Pb^{2+} ions. Fig. 8 shows a change in the peak intensity of UV-vis spectra of Zr-doped ZnONPs after the interaction with different con-

TABLE-2
UV-VIS ANALYSIS OBSERVATION OF Zr-DOPED ZnONPs WITH DIFFERENT METAL IONS

Analyte/toxin (with Zr-doped ZnONPs solution)	Observation in UV-vis spectrum	Sensitivity	Possible interaction mechanism
Pb^{2+}	Significant increase in the visible range and distinct absorption in the UV range	High	As a result of surface absorption on NPs and charge transfer, leading to the formation of a defect state
Hg^{2+}	No significant changes	Low	Minimum surface interaction with NPs
Cd^{2+}	No significant changes	Low	Minimum surface interaction with NPs
As^{3+}	No significant changes	Low	Minimum surface interaction with NPs
Cr^{3+}	No significant changes	Low	Minimum surface interaction with NPs
Cu^{2+}	No significant changes	Low	Minimum surface interaction with NPs
Mg^{2+}	No significant changes	Low	Minimum surface interaction with NPs
Cr^{6+}	No significant changes	Low	Minimum surface interaction with NPs
KCl	No significant changes	Low	Minimum surface interaction with NPs
Ni^{2+}	No significant changes	Low	Minimum surface interaction with NPs
Ca^{2+}	No significant changes	Low	Minimum surface interaction with NPs

centrations of Pb^{2+} ions. A hypochromic shift was observed with an increase in the concentration of Pb^{2+} ions from 0.01 to 10 ppm as shown in Fig. 8. These results confirm the excellent selectivity of the synthesized Zr-doped ZnONPs in the aqueous systems. This confirms the limit of detection of the synthesized Zr-doped ZnONPs is 0.1 ppm, making it appropriate for quantitative detection of Pb^{2+} ions in aqueous system.

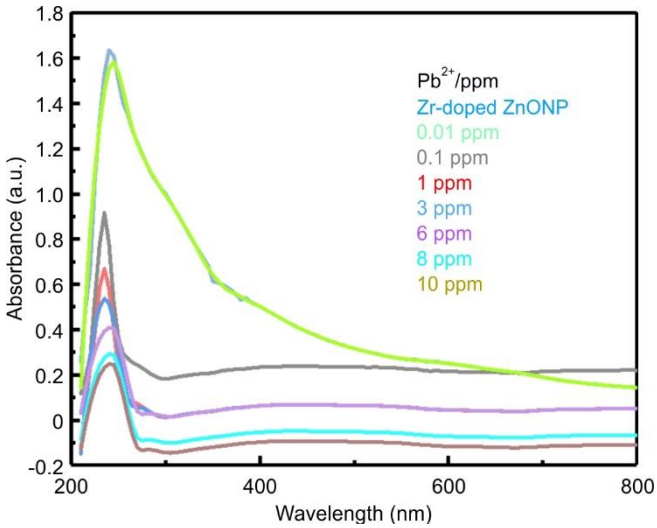

Fig. 8. UV-vis spectra of Zr-doped ZnONPs at different Pb^{2+} ions concentrations (0.01-10 ppm

Practical application: Fig. 9a displays the UV-vis spectrum of the Saryu River water sample. No satisfactory peaks can be seen from this graph. The Saryu River's water was used to prepare a 100 ppm solution of Pb^{2+}, Cr^{3+}, Hg^{2+}, As^{3+}, Cd^{2+}, Cu^{2+}, Ca^{2+}, Cr^{6+}, Mg^{2+}, KCl and Ni^{2+} each. Fig. 9b displays the UV-vis spectrum of heavy metals in the Saryu River water sample when the Zr-doped ZnONPs were introduced. The Pb^{2+} shows a distinct absorbance pattern, making a hyperchromic shift at 230 nm and a bathochromic 390 nm shift as observed in Fig. 9c, indicating potential interaction between these materials and Zr-doped ZnONPs in the visible region. On the addition of Zr-doped ZnONPs to Pb^{2+}, the wavelength increased, which means the energy band gap decreased and thus may hinder the transition. The remaining materials show a similar absorbance pattern to Zr-doped ZnONPs. This test approves the high sensitivity of Zr-doped ZnONPs towards Pb^{2+} ions. The UV-vis test results can be seen in Table-3. Slight changes in the UV-vis peaks can also be observed in Cu^{2+} due to the components present in the Saryu River water sample.

Conclusion

ZnO nanoparticles (ZnONPs) were successfully synthesized and subsequently doped with Zr^{4+} ions. The materials were characterized using SEM, XRD, EDX, UV-visible spectroscopy and FT-IR analysis. The absorption wavelength of the synthesized ZnONPs was observed at 239 nm, which shifted to 230 nm after doping, indicating a change in the optical properties. FT-IR analysis of ZnONPs showed a characteristic ZnO peak at 827 cm^{-1}, while the appearance of an additional peak at 468 cm^{-1} confirmed the successful synthesis of Zr-doped ZnONPs. XRD analysis further verified the presence of ZnO phases in the doped samples. A comparative

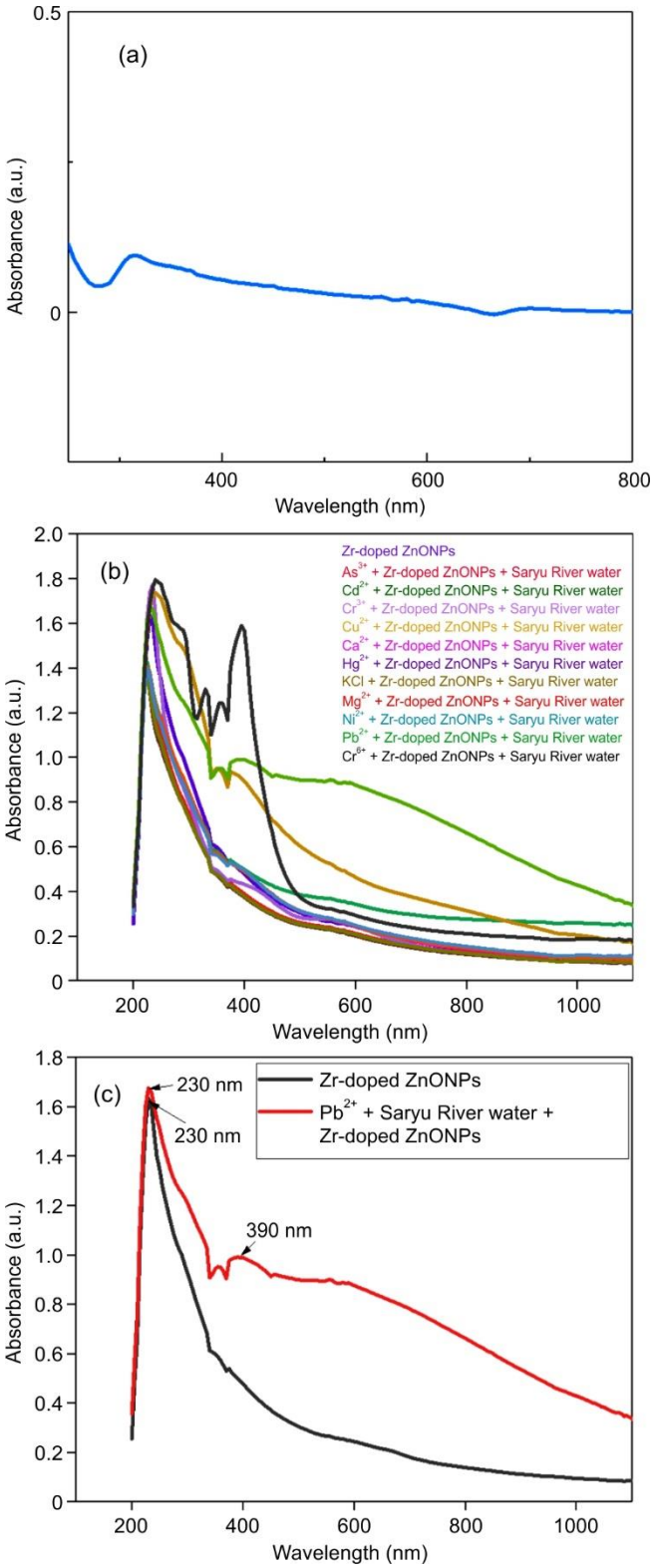

Fig. 9. UV-vis spectrum of (a) Saryu River water; (b) Zr-Doped ZnONPs in the presence of various metal ions solution in Saryu River water (100 ppm each); (c) Zr-Doped ZnONPs with 100 ppm Pb^{2+} solution in Saryu River water

study of pure and Zr-doped ZnONPs demonstrated enhanced selectivity toward heavy and toxic metals, with the doped nanoparticles showing superior performance, particularly at lower concentrations. The minimum detection limit for Pb^{2+}

TABLE-3
UV-VIS ANALYSIS OBSERVATIONS OF Zr-Doped ZnONPs IN SARYU RIVER WATER SAMPLE

Analyte/toxin	Observation in UV-vis spectrum	Sensitivity	Possible interaction mechanism
Pb^{2+}	Significant increase in the visible range and distinct absorption in the UV range	High	As a result of surface absorption on NPs and charge transfer, leading to the formation of a defect state
Hg^{2+}	No change	Low	Minimum surface interaction with NPs
Cr^{3+}	No change	Low	Minimum surface interaction with NPs
Cd^{2+}	No change	Low	Minimum surface interaction with NPs
As^{3+}	No change	Low	Minimum surface interaction with NPs
Mg^{2+}	No change	Low	Minimum surface interaction with NPs
Ca^{2+}	No change	Low	Minimum surface interaction with NPs
Cu^{2+}	Slight changes	Medium	Minimum surface interaction with NPs
Cr^{6+}	No change	Low	Minimum surface interaction with NPs
KCl	No change	Low	Minimum surface interaction with NPs
Ni^{2+}	No change	Low	Minimum surface interaction with NPs

ions using Zr-doped ZnONPs was determined to be 0.1 ppm in aqueous solutions. In practical applications, Zr-doped ZnO NPs exhibited high sensitivity toward Pb^{2+} ions, suggesting their potential for further development in heavy metal sensing technologies.

ACKNOWLEDGEMENTS

The authors thank the Division of Research and Innovation, Uttaranchal University, for providing support to carrying the SEM, EDX and XRD analysis.

CONFLICT OF INTEREST

The authors declare that there is no conflict of interests regarding the publication of this article.

REFERENCES

1. Z.L. Wang, *J. Phys.: Condens. Matter*, **16**, R829 (2004); https://doi.org/10.1088/0953-8984/16/25/R01
2. H. Mirzaei and M. Darroudi, *Ceram. Int.*, **43**, 907 (2017); https://doi.org/10.1016/j.ceramint.2016.10.051
3. F.T. Thema, E. Manikandan, M.S. Dhlamini and M.J.M.L. Maaza, *Mater. Lett.*, **161**, 124 (2015); https://doi.org/10.1016/j.matlet.2015.08.052
4. N. Singh, S.P. Singh, V. Gupta, H.K. Yadav, T. Ahuja, S.S. Tripathy and Rashmi, *Environ. Prog. Sustain. Energy*, **32**, 1023 (2013); https://doi.org/10.1002/ep.11698
5. M.I. Hussain, N.A. Rahman, H. Dutta, D. Dutta and R.R. Dutta, *Next Sustainability*, **5**, 100129 (2025); https://doi.org/10.1016/j.nxsust.2025.100129
6. Bharti, J.S. Jangwan, G. Kumar, V. Kumar and A. Kumar, *SN Appl. Sci.*, **3**, 311 (2021); https://doi.org/10.1007/s42452-021-04294-0
7. J. Jiang, J. Pi and J. Cai, *Bioinorg. Chem. Appl.*, **1**, 1062562 (2018); https://doi.org/10.1155/2018/1062562
8. S. Raut, D.P. Thorat and R. Thakre, *Int. J. Sci. Res.*, **4**, 1225 (2015).
9. K. Qi, X. Xing, A. Zada, M. Li, Q. Wang, S.-Y. Liu, H. Lin and G. Wang, *Ceramics Int.*, **46**, 1494 (2020); https://doi.org/10.1016/j.ceramint.2019.09.116
10. S.J. Pearton, D.P. Norton, K. Ip, Y.W. Heo and T. Steiner, *Superlattices Microstruct.*, **34**, 3 (2003); https://doi.org/10.1016/S0749-6036(03)00093-4
11. E.I. Naik, H.S.B. Naik, R. Viswanath, B.R. Kirthan and M.C. Prabhakara, *Chemical Data Coll.*, **29**, 100505 (2020); https://doi.org/10.1016/j.cdc.2020.100505
12. K. Nagaraj, R. Kaliyaperumal, V.K. Poovan, M.K. Al-Sadoon, T. Kasilingam and K. Tharini, *J. Indian Chem. Soc.*, **101**, 101386 (2024); https://doi.org/10.1016/j.jics.2024.101386
13. A. R. Khan, M. Ramzan, M. Imran, M. Zubair, S. Shahab, S.J. Ahmed, F. Ferreira and M.F. Iqbal, *Coatings*, **13**, 34 (2022); https://doi.org/10.3390/coatings13010034
14. V. Gokulakrishnan, S. Parthiban, K. Jeganathan and K. Ramamurthi, *Appl. Surf. Sci.*, **257**, 9068 (2011); https://doi.org/10.1016/j.apsusc.2011.05.102
15. M. Sathya, G. Selvan, K. Kasirajan, S. Usha, P. Baskaran and M. Karunakaran, *J. Mater. Sci. Mater. Electron.*, **33**, 443 (2022); https://doi.org/10.1007/s10854-021-07318-y
16. G. Algün and N. Akçay, *Phys. Scr.*, **100**, 085902 (2025); https://doi.org/10.1088/1402-4896/adeedd
17. N. Ullah, M. Mansha, I. Khan and A. Qurashi, *Trends Analyt. Chem.*, **100**, 155 (2018); https://doi.org/10.1016/j.trac.2018.01.002
18. R. Verma, S. Pathak, A.K. Srivastava, S. Prawer and S. Tomljenovic-Hanic, *J. Alloys Compd.*, **876**, 160175 (2021); https://doi.org/10.1016/j.jallcom.2021.160175
19. M. Iftikhar, M. Zahoor, S. Naz, N. Nazir, G.E.S. Batiha, R. Ullah, A. Bari, M. Hanif and H.M. Mahmood, *J. Nanomater.*, **2020**, 8949674 (2020); https://doi.org/10.1155/2020/8949674
20. G. Uddin, W. Ullah, B.S. Siddiqui and S.Q. Shah, *Nat. Prod. Res.*, **27**, 215 (2013); https://doi.org/10.1080/14786419.2012.666749
21. S.M. Salman, M. Wahab, M. Zahoor, D. Shahwar, S. Sultana, M. Alamzeb and S. Ahmed, *Desalination Water Treat.*, **195**, 413 (2020); https://doi.org/10.5004/dwt.2020.25904
22. S. Arora, *J. Pharm. Res.*, **4**, 9 (2011).
23. A. Ahmed, A. Singh, B. Padha, A.K. Sundramoorthy, A. Tomar and S. Arya, *Chemosphere*, **303**, 135208 (2022); https://doi.org/10.1016/j.chemosphere.2022.135208
24. S.W. Balogun, O.O. James, Y.K. Sanusi and O.H. Olayinka, *SN Appl. Sci.*, **2**, 504 (2020); https://doi.org/10.1007/s42452-020-2127-3
25. A. Gupta, P. Srivastava, L. Bahadur, D.P. Amalnerkar and R. Chauhan, *Appl. Nanosci.*, **5**, 787 (2015); https://doi.org/10.1007/s13204-014-0379-1
26. S. Gouthamsri, M. Ramanaiah, K. Basavaiah and K.J. Rao, *Results Chem.*, **6**, 101080 (2023); https://doi.org/10.1016/j.rechem.2023.101080
27. J.A. Ibrahim, S. Rajasekar and M. Varsha, *Glob. NEST J.*, **23**, 526 (2021).
28. S.W. Jin, G.H. Lee, J.Y. Kim, C.Y. Kim, Y.M. Choo, W. Cho, J.H. Choi, E.H. Han, Y.P. Hwang and H.G. Jeong, *Appl. Sci.*, **12**, 17 (2021); https://doi.org/10.3390/app12010017
29. O.M. El-Borady and A.F. El-Sayed, *J. Mater. Res. Technol.*, **9**, 1905 (2019); https://doi.org/10.1016/j.jmrt.2019.12.02
30. I. Khan, S. Khan, R. Nongjai, H. Ahmed and W. Khan, *Opt. Mater.*, **35**, 1189 (2013); https://doi.org/10.1016/j.optmat.2013.01.019
31. S.C. Liufu, H.N. Xiao and Y.P. Li, *Polym. Degrad. Stab.*, **87**, 103 (2005); https://doi.org/10.1016/j.polymdegradstab.2004.07.011
32. S. Bashir, M. Awan, M.A. Farrukh, R. Naidu, S.A. Khan, N. Rafique, S. Ali, I. Hayat, I. Hussain and M.Z. Khan, *Int. J. Nanomedicine*, **17**, 4073 (2022); https://doi.org/10.2147/IJN.S372343

33. S. Alamdari, M. Sasani Ghamsari, C. Lee, W. Han, H.H. Park, M.J. Tafreshi, H. Afarideh and M.H.M. Ara, *Appl. Sci.*, **10**, 3620 (2020); https://doi.org/10.3390/app10103620
34. B. Abderrahim, E. Abderrahman, A. Mohamed, T. Fatima, T. Abdesselam and O. Krim, *World J. Environ. Eng.*, **3**, 4 (2015); https://doi.org/10.12691/wjee-3-4-1
35. R. Ali, Z. Aslam, R.A. Shawabkeh, A. Asghar and I.A. Hussein, *Turk. J. Chem.*, **44**, 279 (2020); https://doi.org/10.3906/kim-1909-20
36. D.S. Raju, S.H. Bindu, J.S. Krishna, V.V. Krishna and C.L. Raju, *J. Phys. Conf. Ser.*, **1913**, 012011 (2021); https://doi.org/10.1088/1742-6596/1913/1/012011
37. M. Ashokkumar and S. Muthukumaran, *Opt. Mater.*, **37**, 671 (2014); https://doi.org/10.1016/j.optmat.2014.08.012
38. A. Azam, F. Ahmed, N. Arshi, M. Chaman and A.H. Naqvi, *J. Alloys Compd.*, **496**, 399 (2010); https://doi.org/10.1016/j.jallcom.2010.02.028
39. S.B. Patel, N. Baker, I. Marques, A. Hamlekhan, M.T. Mathew, C. Takoudis, C. Friedrich, C. Sukotjo and T. Shokuhfar, *RSC Adv.*, **7**, 30397 (2017); https://doi.org/10.1039/C7RA03940A
40. G.K. Sidhu, A.K. Kaushik, S. Rana, S. Bhansali and R. Kumar, *Appl. Surf. Sci.*, **334**, 216 (2015); https://doi.org/10.1016/j.apsusc.2014.10.036
41. E.I. Naik, H.B. Naik, R. Viswanath, B.R. Kirthan and M.C. Prabhakara, *Chemical Data Coll.*, **29**, 100505 (2020); https://doi.org/10.1016/j.cdc.2020.100505
42. G. Murtaza, R. Ahmad, M.S. Rashid, M. Hassan, A. Hussnain, M.A. Khan, M. Ehsan ul Haq, M.A. Shafique and S. Riaz, *Curr. Appl. Phys.*, **14**, 176 (2014); https://doi.org/10.1016/j.cap.2013.11.002
43. H.R. Mardani, M. Forouzani, M. Ziari and P. Biparva, *Spectrochim. Acta A Mol. Biomol. Spectrosc.*, **141**, 27 (2015); https://doi.org/10.1016/j.saa.2015.01.034
44. H.S. Abbas, A. Krishnan and M. Kotakonda, *Front. Bioeng. Biotechnol.*, **8**, 595161 (2020); https://doi.org/10.3389/fbioe.2020.595161
45. T. Arfin and A. Tarannum, *J. Environ. Chem. Eng.*, **7**, 102811 (2019); https://doi.org/10.1016/j.jece.2018.102811
46. H. Akhtar, F.H. Alhamoudi, J. Marshall, T. Ashton, J.A. Darr, I.U. Rehman, A.A. Chaudhry and G. Reilly, *Heliyon*, **10**, e20150 (2024); https://doi.org/10.1016/j.heliyon.2024.e29150
47. E.J.S. Christy, A. Amalraj, A. Rajeswari and A. Pius, *Environ. Chem. Ecotoxicol.*, **3**, 31 (2021); https://doi.org/10.1016/j.enceco.2020.10.005
48. V. Mariyappillai, C. Shiyamala, T. Abisheik, M. Tiffany, V. Pandiyan, A. Senthilraja, M. Afzal, P. Barmavatu, K. Shanmugaraj and K. Balu, *Ceram. Int.*, **51**, 23003 (2025); https://doi.org/10.1016/j.ceramint.2025.02.402
49. M.E. Mahmoud, G.M. Nabil and S.M. Mahmoud, *J. Environ. Chem. Eng.*, **3**, 1320 (2015); https://doi.org/10.1016/j.jece.2014.11.027
50. Y. Luo and F.J. Millero, *Geochim. Cosmochim. Acta*, **71**, 326 (2007); https://doi.org/10.1016/j.gca.2006.09.019